Scalar Calibration for Broadband Synthetic Aperture Radar Operating with Amplitude-Only Data

Jaime Laviada and Fernando Las-Heras, *Senior Member, IEEE*

***Abstract*—Off-axis holography techniques, which are commonly used to perform phase retrieval from amplitude-only data, require a full-characterization of the reference signal in terms of amplitude and phase. In this letter, it is demonstrated that the recently proposed version of the off-axis holography, working with a broadband synthetic aperture radar, can bypass the need for this calibration. The strategy is based on employing a calibration object to adjust the system. Furthermore, certain properties of the reflectivity calculation are exploited to correct potential misalignment errors. The performance of the approach is demonstrated by reconstructing the profile of several objects at K_a-band.**

***Index Terms*—Synthetic aperture radar; Leith-Upatnieks; indirect holography; phase retrieval.**

I. Introduction

AMPLITUDE or power acquisition usually involves a technological complexity lower than a full acquisition involving amplitude and phase. Nevertheless, both quantities are usually required in most of *postprocessing techniques* (e.g., backpropagation, far-field computation, etc.). These facts have motivated a large number of works to retrieve the phase from *amplitude-only data*. The most widespread techniques are the acquisition at two or more different acquisition surfaces [1], [2] and the use of *off-axis holography* [3], [4]. The reader is referred to [5] for a summary on these and other phase retrieval techniques.

Recently, a novel methodology [5] based on off-axis holography has been proposed for the case of a synthetic aperture radar (SAR) relying on multi-monostatic acquisition. Although this technique benefits from the non-iterative technique nature of the off-axis holography and, therefore, it does not suffer from stagnation problems (e.g., [1]), it also inherits some of the disadvantages. For example, an initial *vector calibration* of the system must be accomplished because some signals must be characterized in terms of amplitude and phase.

The main contribution of this letter is a *scalar calibration* for the phaseless SAR proposed in [5] by means of a reference object. Thus, the resulting system becomes completely independent of any vector measurement. In addition, the robustness of the calibration is enhanced by taking advantage of certain properties of the reflectivity computation to correct any possible *misalignment*.

This work has been supported by the Ministerio de Ciencia e Innovación of Spain /FEDER under projects TEC2011- 24492 (iScatt), CSD2008-00068 (Terasense) and MICINN-11-IPT-2011-0951-390000 (Tecnigraf); by the Ministerio de Economía y Competitividad under postdoctoral fellowship FPDI-2013-16278; by the Gobierno del Principado de Asturias (PCTI)/FEDER-FSE under project GRUPIN14-114.

Jaime Laviada is with the Departamento de Ingeniería Eléctrica y Electrónica de la Universidad Pública de Navarra, Spain (e-mail: jaime.laviada@unavarra.es). Fernando Las-Heras is with the Departamento de Ingeniería Eléctrica, Universidad de Oviedo, Spain (e-mail: flasheras@uniovi.es)

II. Broadband off-axis holography

A. Phase retrieval

Time-domain off-axis holography works in a similar fashion to conventional off-axis holography by translating the concepts from the spatial/spectral domains to the frequency/time domains [5]. Thus, this technique involves acquiring the power of the signal that results of combining the scattered field with a reference field:

$$I(\vec{r},\omega) = |E_S(\vec{r},\omega) + R(\vec{r},\omega)|^2, \quad (1)$$

where E_S is the signal acquired by the receiver antenna associated with the scattered field at each position of the quasi-monostatic scanning element and R is the reference signal, whose amplitude and phase must be characterized in a previous *calibration stage*. The goal of this holographic technique is to retrieve the phase of E_S from the knowledge of the reference field as well as the amplitude of I and E_S.

As detailed in [5], if the energy of the reference signal is contained in a narrow window in the time domain, then the amplitude and phase of the scattered field can be retrieved by time gating the *modified hologram* [5], which is computed by subtracting $|E_S(\vec{r},\omega)|^2$ and $|R(\vec{r},\omega)|^2$ from (1).

The schematic circuit to obtain the hologram in (1), which includes standard components such as directional couplers and power combiners, is described in Fig. 1 in [5].

The reference signal can be usually approximated by a delayed and attenuated signal:

$$R(\vec{r},\omega) = C(\vec{r})\, e^{-j\omega t_d}, \quad (2)$$

where t_d models the delay of the signal through the reference branch [5] and C is a positive real value modeling the attenuation. In general, this last parameter is controlled by a variable attenuator to balance the power of the two signals in (1). Further details on the delay t_d and the attenuation C, are given in [5].. Hence, the calibration of the algorithm can be reduced to the computation of these *two parameters*. Although the last one can be retrieved by means of a scalar measurement, the first one requires a vector measurement. In order to bypass this last measurement, an algorithm based on scalar measurement is proposed in this letter. However, some properties of the profile reconstruction algorithms, which are useful for the calibration, will be firstly presented in the next section.

B. Impact of the phase retrieval on the reflectivity calculation

The two-dimensional reflectivity of an object, and so its profile reconstruction, can be calculated from the field acquired at a single frequency ω_0 by means of the following expression [6]:

$$S_{2D}(x,y,z_0) = \mathcal{F}^{-1}\left(\mathcal{F}\left(E_S(x,y,\omega_0)\right)e^{-jk_z.z_0}\right), \quad (3)$$

wherein z_0 is the distance from the antenna phase center to the object under test (OUT), the operator $\mathcal{F}$ denotes Fourier transform and k_z is the wavenumber for the z-axis that depends on the angular frequency ω_0 (see [6] for further details).

Next, it will be proved that the phase of the reference signal is *not* required to properly accomplish the computation of the 2D reflectivity. Let us consider that the reference field is set to an arbitrary delay value $\tilde{t}_d$ so the estimated reference field is given by:

$$\tilde{R} = C(\vec{r})\, e^{-j\omega\tilde{t}_d}. \quad (4)$$

Since the expression (1) can be reformulated as:

$$\begin{aligned} I(\vec{r},\omega) &= \left|E_S(\vec{r},\omega) + R(\vec{r},\omega)\right|^2 \\ &= \left|E_S(\vec{r},\omega)\, e^{j\omega\left(t_d-\tilde{t}_d\right)} + R(\vec{r},\omega)\, e^{j\omega\left(t_d-\tilde{t}_d\right)}\right|^2 \\ &= \left|E_S(\vec{r},\omega)\, e^{j\omega\left(t_d-\tilde{t}_d\right)} + \tilde{R}(\vec{r},\omega)\right|^2, \end{aligned} \quad (5)$$

consequently, the scattered field retrieved by the phase retrieval algorithm is given by:

$$\tilde{E}_S(\vec{r},\omega) = E_S(\vec{r},\omega)\, e^{j\omega\left(t_d-\tilde{t}_d\right)}, \quad (6)$$

and, therefore, if only the reconstruction *at a given frequency* ω_0 is considered, then both fields only differ on a *phase constant* $e^{j\omega_0\left(t_d-\tilde{t}_d\right)}$. According to (3) and (6), an arbitrary estimation of the phase of the reference field will only result in the multiplication of the reflectivity by a (possibly) unknown constant. Since profile reconstruction only requires the amplitude of the reflectivity, then this reconstruction is not affected by an arbitrary estimation of the phase of the reference field.

On the other hand, three dimensional reconstruction as given in [6] requires the phase dependence on the frequency and, consequently, the reference field must be accurately estimated. Moreover, the retrieved phase of the scattered field must be referred to the *phase center of the antennas* in order to apply the profile reconstruction algorithms [6]. Since the circuitry for the amplitude-only SAR detailed in [5] requires several components (e.g., a directional coupler and a power combiner), some delay is also introduced. In practice, the field can be referenced to the phase center of the antennas by multiplying E_s by an exponential function to compensate the extra delay. Consequently, it can be considered that a fair model for the reference signal is given by:

$$R'(\vec{r},\omega) = C(\vec{r})\, e^{-j\omega(t_d-t_c)} = C(\vec{r})\, e^{-j\omega t_e}, \quad (7)$$

where t_c is a constant to compensate the propagation through the different components (e.g., directional coupler, variable attenuator, etc.). If an *effective delay* is defined as $t_e = t_d - t_c$, then the full calibration of the system is reduced to the calculation of this parameter.

In the next section, it will be shown how the two-dimensional and three-dimensional reconstructions of a *calibration object* can be exploited to accurately retrieve this effective delay.

C. Scalar calibration algorithm

The algorithm to automatically adjust the system relies on measuring the field scattered by a *calibration object*. A set of parameters including alignment errors in the real position of the calibration object and, of course, the effective delay t_e. Each combination of values for the aforementioned parameters yields a different estimation of the calibration object profile estimated by the imaging algorithms provided in [6]. These profiles are compared with the theoretical one to find the best estimation of the parameters under consideration.

The calibration process is accomplished in two stages. The first stage involves a *two-dimensional reconstruction* and it takes advantage of the immunity to the error in the estimation of the phase of the reference signal. Thus, *alignment errors* concerning the XY plane and the *distance* z_0 can be detected without considering the phase of the reference signal yet. Although it has not been considered in the herein presented implementation, a similar methodology could be considered to detect rotations of the calibration object with respect to the z-axis. In this stage, the two dimensional *fitness function* to be maximized is defined by the following dot product:

$$f_{2D}(\vec{r}_{xy}, z_0) = \bar{M}_{2D}(\vec{r}_{xy}) \cdot \bar{P}_{2D}(z_0), \quad (8)$$

wherein $\bar{M}(\vec{r}_{xy})$ is a vector containing the samples of the 2D mask representing the object with an offset $\vec{r}_{xy}$ with respect to the center (see Fig. 1a for an example of the borders of the mask). This mask is binary and takes the value of *one* inside the profile of the reference object and *minus one* outside this profile. The vector $\bar{P}_{2D}(z_0)$ contains the samples of the 2D reconstructed profile rearranged also as a 1D vector. This profile is computed by setting to one the pixels of the reflectivity S_{2D} over a given threshold. Otherwise, the pixels of the reconstructed profile are set to zero. It is interesting to observe that other phaseless techniques have also considered misalignment errors as for example those based on acquiring the field at multiple surfaces [2].

The two-dimensional reconstruction must be accomplished at the highest available frequency because it provides the best resolution. Regarding this point, it is important to bear in mind that the phase retrieval algorithm returns a scattered field which is contaminated by strong error at the first and last frequencies that must be consequently discarded [5].

Since this process involves a two-dimensional reconstruction, the calibration object is recommended to be *flat*. It is also recommended to choose a calibration object that exhibits a *sharp* profile reconstruction. In order to improve this sharpness, it is recommended that the dimensions are in the order of a few wavelengths as well as to use a material with a high contrast with respect to the supporting material (e.g., a metallic object supported by foam).

Once the distance z_0 and the offset $\vec{r}_{xy}$ have been estimated, the second step, which entails *three-dimensional reconstruction*, is accomplished. In this case, different effective *time*

delays are sequentially considered to find the best matching with a three-dimensional mask that it is placed according to the position given by z_0 and $\vec{r}_{xy}$ estimated in the first step. The thickness of this mask is proportional to the theoretical depth resolution [6], which is given by $\rho = c/2B$, being B the bandwidth of the acquisition. In a similar fashion to the previous case, the fitness function for this stage is given by:

$$f_{3D}(t_e) = \bar{M}_{3D}\left(\vec{r}_{xy}, z_0, \rho\right) \cdot \bar{P}_{3D}\left(t_e\right), \tag{9}$$

wherein $\bar{M}_{3D}$ and $\bar{P}_{3D}$ are vectors containing the values of the voxels corresponding to the 3D mask and the 3D profile. These two vectors are equivalent to those corresponding to two-dimensionals quantities of the first calibration stage.

In both stages, the search of the maximum of the fitness function is based on evaluating *all* the points inside a grid with all the possible values. Although more refined optimization approaches could be used, this brute force approach is preferred because the number of parameters for each stage is very low (two parameters in the first stage and one in the second stage). Moreover, these parameters will be always inside a limited range because misalignment error and time delay cannot take any arbitrary value. Finally, the evaluation of the reflectivity for each combination is very fast as it is based on Fourier transforms [6]. Consequently, the overall optimization process can be performed in the order of a few minutes in modern computers.

III. Measurements Results

In order to validate the scalar calibration algorithm, the quasi-monostatic setup described in [5] has been implemented working in the Ka-band from 26.5 GHz to 40 GHz. The number of frequencies is set to 101 but the first and last five frequencies are discarded after the phase retrieval since they are strongly contaminated by error as previously mentioned.

A. Calibration

In order to calibrate the system, a square aluminum plate with a hole in the center has been used. The edge of the plate is 10 cm and the diameter of the hole is 3 cm. This calibration object is shown in Fig. 1 together with the mechanical arm which is used to move the object along the scanning surface. Masking tape is used to fix the calibration object to a foam support that exhibits low electromagnetic reflections.

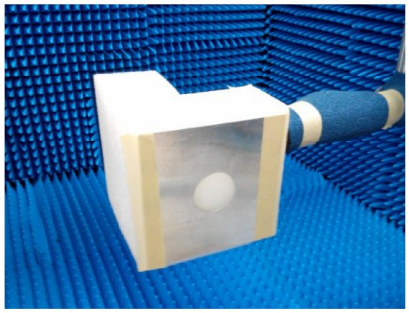

Figure 1. Calibration object fixed on a foam support.

The object is scanned in a plane with dimensions 20 cm × 20 cm with a increment of $\Delta x = \Delta y = \lambda_{min}/4$ wherein λ_{min} is the wavelength at the maximum working frequency (40 GHz). The calibration object is placed at a distance of 23 cm far from the aperture of the antennas.

To carry out the first stage of the calibration, the threshold to compute the object profile from the normalized 2D reflectivity was fixed to −5 dB. The algorithm was requested to search for the best focused image in the range from $z = 21$ cm to $z = 27$ cm. At each distance, the mask was moved along the entire image plane to detect the position inside the XY plane. The algorithm detects the best focused image at $z_0 = 22.8$ cm that agrees well with the real distance. The results corresponding to this distance as well as the mask marking the position of the object are shown in Fig. 2a. It is also important to notice that the position of the object was affected by a small offset with respect to the center of the image plane of 0.2 cm and 0.5 cm in the x- and y-axis respectively. This offset was also correctly detected as it is inferred from the position of the mask in Fig. 2a.

The second stage of the calibration is accomplished by sweeping the effective delay from 48 ns to 90 ns. The threshold to compute the object profile is also fixed to −5 dB of the normalized reflectivity. According to the previous threshold, it has been observed that a fair estimation of the mask thickness is 0.6ρ.

The optimal point is found at $t_e = 72$ ns. The three-dimensional image of the calibration object for the previous value is shown in Fig. 2b revealing an excellent performance of the reconstruction algorithm.

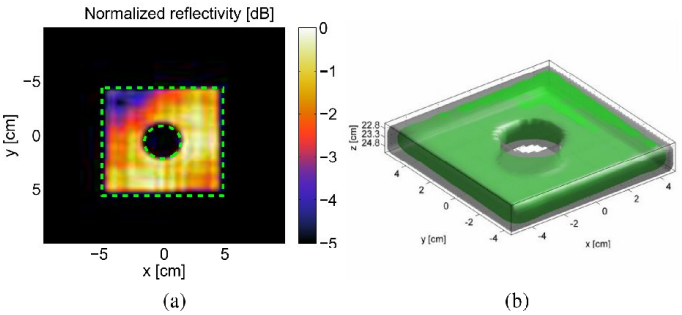

Figure 2. Reflectivity of the calibration object and mask enclosing the reconstruction: a) 2D profile after the first calibration step; b) 3D profile with −5 dB threshold after the second calibration step.

B. Profile reconstruction from scalar calibration

Once the reference signal has been estimated, the reconstruction of 3D objects becomes possible by applying standard reflectivity calculations [6].

The OUT corresponding to the first example is shown in Fig. 3. This object is composed of two metallic plates held by a support built by a 3D printer and it is placed at 23 cm from the aperture of the antennas and scanned along a plane of dimensions 19.76 cm × 19.76 cm.

The results of the reconstruction are shown in Fig. 4 for two different reflectivity thresholds. Results achieved by considering the full, i.e., the amplitude and phase, acquired data (repeating the steps in [5]) are also shown to provide a reference result. Despite the lack of a calibration based on vector measurements, the system is clearly able to provide

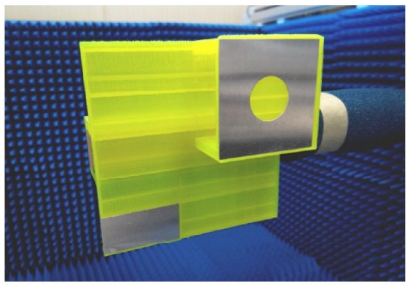

Figure 3. Composite OUT with metal and dielectric parts.

very accurate results. Furthermore, the capacity of the system to discern between metallic and dielectric regions by changing the reflectivity threshold is not affected.

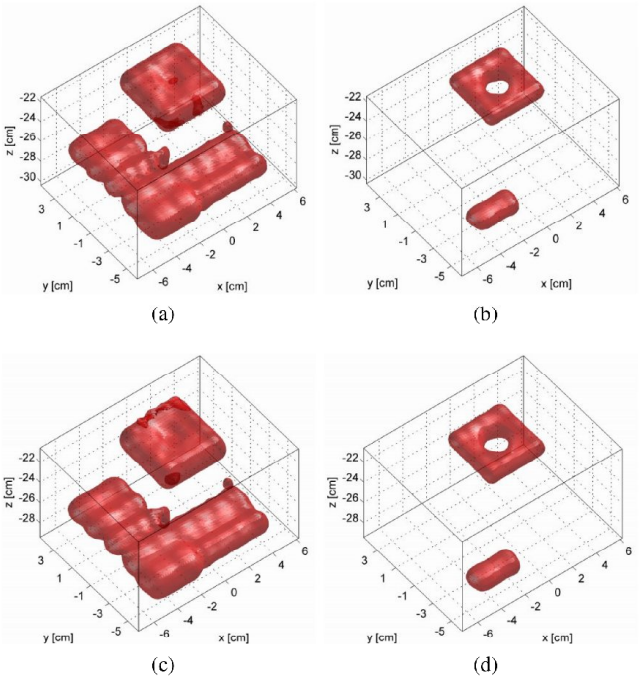

Figure 4. Reconstruction of an object composed of metal and dielectric for two different thresholds: a) phaseless acquisition and scalar calibration with threshold at $-12\,\mathrm{dB}$; b) phaseless acquisition and scalar calibration with threshold at $-5\,\mathrm{dB}$; c) full acquisition and threshold at $-12\,\mathrm{dB}$; d) full acquisition and threshold at $-5\,\mathrm{dB}$.

In the second example, the capacity of the system to inspect embedded objects is tested. In particular, the scissors shown in Fig. 5 packed in a cardboard box have been scanned. Additional packing materials such as bubble wrap and foam are also used. The packing box was placed at 20 cm from the antenna aperture and the raster scan was accomplished in a plane of dimensions $28.31\,\mathrm{cm} \times 25.46\,\mathrm{cm}$.

The obtained results for the reflectivity isosurface corresponding to $-12\,\mathrm{dB}$ are shown in Fig. 6 where the scissors profile is clearly visible.

IV. Conclusions

The capability to perform broadband SAR acquisitions without the need of any vector measurement has been demonstrated in this letter. The approach relies on novel broadband off-axis holography that enables to implement a multi-monostatic acquisition based on intensity measurements.

Figure 5. Scissors and packaging before closing the cardboard box.

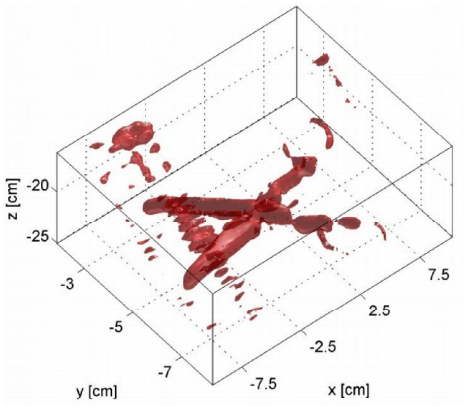

Figure 6. Scissors reconstruction from calibrated phaseless setup. Reflectivity threshold fixed to $-12\,\mathrm{dB}$.

To completely bypass the need of any full acquisition (i.e., amplitude and phase acquisition), a calibration based on the reconstruction of a reference object has been proposed. Moreover, some properties of the reflectivity computation have been employed to improve the robustness against misalignment errors.

Whereas the approach simplifies any scanning system based on SAR, it is considered of special interest for high frequencies (e.g., THz) where phase acquisition becomes specially challenging.

References

[1] T. Isernia, F. Soldovieri, G. Leone, and R. Pierri, "On the local minima in phase reconstruction algorithms," *Radio Science*, vol. 31, no. 6, pp. 1887–1899, Nov-Dec 1996.

[2] A. Capozzoli, C. Curcio, A. Liseno, and P. Vinetti, "An approach for restoring the coherence between the scanning surfaces in phaseless near-field antenna characterization," *Int. J. Electron. Commun. (AEÜ)*, vol. 66, pp. 636–640, 2012.

[3] A. Tamminen, J. Ala-Laurinaho, and A. V. Räisänen, "Imaging with indirect holographic method at 310 GHz," in *Proc. XXXI Finnish URSI Conv. Radio Sci. Electromagn.*, 2008, pp. 31–32.

[4] G. Junkin, T. Huang, and J. Bennett, "Holographic testing of terahertz antennas," *IEEE Trans. Antennas Propag.*, vol. 48, no. 3, pp. 409–417, Mar. 2000.

[5] J. Laviada, Y. Álvarez López, A. Arboleya-Arboleya, C. García-González, and F. Las-Heras, "Phaseless synthetic aperture radar with efficient sampling for broadband near-field imaging: Theory and validation," *IEEE Trans. Antennas Propag.*, no. 2, pp. 573–584, Feb. 2015.

[6] D. M. Sheen, D. L. McMakin, and T. E. Hall, "Three-dimensional millimeter-wave imaging for concealed weapon detection," *IEEE Trans. Microw. Theory Tech.*, vol. 49, no. 9, pp. 1581–1592, Sep. 2001.